Nano Trends 3 (2023) 100014

Contents lists available at ScienceDirect

Nano Trends

journal homepage: www.elsevier.com/locate/nantre

Emperor's new clothes: Novel textile-based supercapacitors using sheep wool fiber as electrode substrate

Alyssa Grube [a], Ahmad Arabi Shamsabadi [b], Mostafa Dadashi Firouzjaei [c], Syed Ibrahim Gnani Peer Mohamed [a], Laurel Hilger [a], Mark Elliott [c], Kaitlin McKenzie [a], Mona Bavarian [a,*]

[a] Department of Chemical and Biomolecular Engineering, University of Nebraska-Lincoln, Lincoln, NE, 68588, UK
[b] Department of Chemistry, University of Pennsylvania, Philadelphia, PA, 19104, USA
[c] Department of Civil, Construction, and Environmental Engineering, University of Alabama, Tuscaloosa, AL, 35487, USA

ARTICLE INFO

Keywords:
Textile-based supercapacitors
MXene
Wool
Highly conductive

ABSTRACT

Textile-based supercapacitors (TSCs) are being used to meet the ever-increasing demand for mobile, safe, and convenient energy sources to power personal electronic devices. To that end, the smart textiles used in wearable technology need to be made from highly conductive yarns that are easily manufacturable. To date, synthetic- and cellulosic-based yarns have been exclusively used for the fabrication of TSCs, while other yarns have not been explored. Here, we used conductive protein-based yarns for TSCs and report on the use of wool coated with $Ti_3C_2T_x$ MXene as a potential electrode material. To knit TSCs, wool and cotton yarns were coated with MXene flakes and their surfaces were characterized using Scanning Electron Microscopy (SEM) and X-Ray Photoelectron Spectroscopy (XPS). The electrochemical characterization was conducted to examine the performance of wool- and cotton-based MXene electrodes as substrates and determine charge storage and resistive behavior. These tests showed that wool TSCs exhibited more pseudocapacitive behavior, while cotton TSCs exhibited a wider current range. At a scan rate of 5 mV/s, cotton TSCs presented an areal capacitance of 823.9 mF/cm^2 while this value for the wool TSCs was 284 mF/cm^2. The performance of yarns was also tested under various mechanical deformation conditions and after washing in order to assess the stability of TSCs. This study indicates the potential of protein-based yarns as electrode substrates for integration of MXene to fabricate smart textile-based devices.

Introduction

For over forty thousand years, humans have been cultivating fibers from plants and animals and processing them into textiles to make clothes. With the advent of more affordable clothing and rapidly changing fashion trends, the demand for clothing has been increasing. [4,7,27] With the technological advances made over the last half a century, devices designed to generate, collect, and store energy are now gaining momentum. [31] In recent years, using clothing to harvest energy from body heat and movement has been viewed as the next logical step toward textile-based electronics. [34] The combination of energy-storage devices with clothing creates power sources that are as mobile as the current generation of personal electronic devices. However, conventional energy storing devices such as capacitors and batteries are too rigid and bulky for their incorporation into clothing. Hence, there is a demand for soft and flexible energy storage devices. [19,29,32]

As a result, several fabrication techniques have been developed to create textile-based electronics for powering personal electronics [33]. One method involves printing circuits onto woven cloth using conductive ink; while printing stiffens the fabric, the clothing is still soft and flexible enough to wear comfortably, as shown by the popularity of graphic T-shirts. [63] A different fabrication method that preserves the flexibility of textiles is to create conductive threads with concentric electrodes out of carbon-based material and conductive polymers, and stitching circuits into cloth. An exciting innovation in the field of textile-based supercapacitors (TSCs) is to create conductive yarns by coating them with conductive materials and knitting circuits with them.

* Corresponding author.
E-mail address: mona.bavarian@unl.edu (M. Bavarian).

https://doi.org/10.1016/j.nwnano.2023.100014
Received 7 May 2023; Received in revised form 3 July 2023; Accepted 11 July 2023
Available online 13 July 2023

This strategy increases the number of contact points the yarn has with itself, reducing the electrode resistance and losses [30,60,61]. In comparison with the printable electronics, TSCs offer superior performance. Among the various materials used to coat the fibers and render them conductive, MXene-based TSCs have gained significant attention from textile and material researchers. [28]

MXenes are conductive two-dimensional (2D) materials with a general chemical formula of $M_{n+1}X_nT_x$, where M is a transition metal carbide, X describes carbon and/or nitrogen, and T represents the surface terminations. [12] While there are many different types of MXenes, $Ti_3C_2T_x$ is the most extensively studied because it is more stable than other MXenes, has a conductivity up to 10,000 S/cm, and excellent volumetric capacitance up to 1500 F/cm^3. [8,38] Furthermore, $Ti_3C_2T_x$ has demonstrated exceptional cation intercalation and pseudocapacitive behavior, excellent anti-microbial activities and non-toxicity when worn on the skin, and it has high hydrophilic and mechanical properties that allow for their excellent solution and textile processability. [2,21,22,24,28,44,47,49,55,62]

While MXene flakes provide an effective conductive coating for yarn, there are challenges associated with the coating. The MXene flakes act like a pigment and stiffen the yarn during the coating process; if the yarn is stiffened too much it can break while knitting circuits. Consequently, smaller MXene flakes are more appropriate to use when coating yarns for knitting textile-based electronics. Additionally, small flakes can penetrate through the yarn and coat individual fibers instead of forming a rigid shell around the yarn. While MXene has satisfactory cycling stability, the material is susceptible to oxidation; upon degradation, TiO_2 and CO_2 are produced. [58] Oxidation can be mitigated by adding antioxidants, and the degradation can be avoided by designing textile-based electronics for short-term use in military expeditions and medical monitoring devices. [24,28,64]

Thus far, TSC research that explores coating yarn with conductive material has exclusively focused on using yarn spun from plant-based or artificial fibers, especially cotton and nylon. Even though these fibers are readily available, there are several drawbacks to this approach. Nylon is made from mined oil that has been chemically treated, and thus its manufacturing contributes to environmental pollution. Even if nylon is produced from recycled plastic, this does not address the plastic microfibers that are released every time nylon is washed, or the fact that the genesis of these materials was mined oil. While cotton is a naturally occurring fiber with good water uptake properties, due to the nature of its cultivation and processing, a substantial amount of polluted water is produced [9,23,48].

In this study, the use of sheep wool as a substrate for conductive materials is reported for the first time. Sheep wool was selected as a substrate for conductive materials because of its availability, sustainability, outstanding water uptake abilities, and insulating properties. As a keratin fiber, sheep wool has several unique properties that make it distinct from other fibers. Keratin fiber has more surface charges compared with cellulosic or synthetic fibers, giving wool its excellent water uptake properties [23,53]. This fiber is more renewable than synthetic or cellulosic yarns because it is continuously grown by sheep that can be sheared multiple times every year for the duration of their lives, whereas other fibers require new crops to be planted or more mined oil in order to produce them. [48]

In this paper, we describe, for the first time, the fabrication of wool-based TSCs. Conductive yarn was created by coating wool yarn with $Ti_3C_2T_x$ MXene flakes. The electrochemical performance of TSCs made of wool coated with $Ti_3C_2T_x$ was evaluated and compared with that of the TSCs made of the $Ti_3C_2T_x$ coated cotton. The coated yarns were characterized using scanning electron microscopy-energy dispersive spectroscopy (SEM-EDS) and X-ray photoelectron spectroscopy (XPS). The electrochemical behavior of $Ti_3C_2T_x$ -coated wool yarns indicate their potential for building smart textile-based devices.

Experimental methods

Materials

Ti_3AlC_2 MAX powder, HF acid (38%), sodium carbonate (99.95%), and ortho-phosphoric acid crystals (99%) used as the electrolyte for electrochemical testing of all TSCs were purchased from Sigma. HCl (37%) and LiCl (99%) were supplied from Fisher Chemical and Alfa Aesar, respectively. Cotton perle yarn, 10/2 pure in white, was purchased from Silk City Fibers. Merino lace-weight wool yarn in ecru was acquired from The Woolery. All TSCs were fabricated on size 0 Takumi 5-inch bamboo double-pointed knitting needles. 1-ply polyester yarn created from recycled polyethylene was supplied from REPREVE, and 85/15 modal/nylon blend in midnight was supplied from Silk City Fibers.

MXene synthesis

Single-layer MXene flakes were produced by mixing 1 g Ti_3AlC_2 MAX powder in a polypropylene bottle with 6 mL DI water, 12 mL HCl, and 2 mL HF. In a silicon oil bath, the mixture was stirred for 24 hours at 35°C. The mixture was centrifuged for 5 min at 3000 rpm to form a centrifuge pellet. Acid was removed by pouring away the supernatant, refilling the centrifuge tubes with DI water and resuspending the pellets before repeating this method until achieving pH of 6. Afterward, 50 mL DI water and 1 g of LiCl were added to the flakes before being suspended in the oil bath at 35°C for 24 hours. A similar washing step was followed, except the tubes were centrifuged for 20 min and the supernatant was checked for opacity; if it was opaque then it was collected for further use.

Yarn preparation

Cotton and wool yarns were wound into hanks weighing 2–4 g. Cotton yarn was scoured in a solution of 2% weight of fiber (WOF) sodium carbonate to remove impurities and hydrolyze the fiber surface to make it hydrophilic. Cotton and wool hanks were dried overnight under continuous vacuum and weighed to determine their dry weight. The hanks were then submerged into a MXene colloidal solution (3.5 mg/mL) and left to soak for one hour to allow the MXene flakes to bind to their surface. The cotton and wool hanks were suspended on a plastic stand and dried under continuously drawn vacuum to remove the DI water, before repeating the coating process. The entire process was repeated 4 times to create MXene-coated cotton and wool yarns.

TSC fabrication

All TSCs were knit by hand using the intarsia knitting technique such that each electrode was 3 stitches wide and 4 stitches tall, separated by 2 stitches. MXene-coated cotton or wool yarn was used for the TSC electrodes, recycled polyethylene yarn was utilized as the electrode separator, and a modal/nylon blend was employed as the fashion yarn surrounding the circuit. TSCs were measured to determine their average area and electrode separation. All TSCs were knit in alternating rows of garter stitch on odd rows and purl stitch on even rows to create a stockinette stitch to approximate the jersey stitch used on machine-knit fabric. All TSCs were made in sextuplicate to generate data for statistical analysis.

Surface characterization

Uncoated and MXene-coated cotton and wool yarns were attached to a sample stand using carbon tape and copper clips before inserting into the Thermo Scientific K-alpha XPS system for collecting XPS spectra. Avantage software was used to run the experiments and analyze the collected data. For uncoated cotton yarn only, carbon and oxygen were scanned, and for MXene-coated cotton yarn titanium and fluoride were

scanned in addition to carbon and oxygen. The uncoated wool yarn was scanned for carbon, oxygen, nitrogen, and sulfur while MXene-coated wool yarn was scanned for these elements in addition to titanium and fluoride. SEM was conducted using a Thermo Fisher Scientific Nova NanoSEM450. Aztec software was used for EDS for elemental analysis of uncoated and MXene-coated cotton and wool yarns.

Electrochemical testing

All TSCs were soaked in 1 M phosphoric acid electrolyte for 10 minutes prior to testing. All TSCs were connected to a Gamry 1000E Potentiostat and characterized in a two-electrode setup for cyclic voltammetry (CV) and electrochemical impedance spectroscopy (EIS).The CV scans of TSCs were performed over a potential range of 0–0.5 V at scan rates of 50, 20, 10, 5, and 2 mV/s. EIS tests were performed in a frequency range of 100 kHz to 0.1 Hz at open circuit potential, by applying a sinusoidal potential signal with an amplitude of 10 mV. Galvanostatic charge/discharge (GCD) tests were performed at current densities ranging from 0.5 to 5 mA/cm^2 to determine cycle life and further characterize the electrodes. In order to determine cycle life, GCD curves were then cycled for 1000 cycles. Before conducting any experiment, the TSC dimensions were measured to determine initial area and electrode spacing.

Effect of washing and mechanical deformation on electrochemical performance

To examine the effect of mechanical stretching, TSCs were then stretched along their course to 1.3 times their width, and along their wale to 1.2 times their length and anchored into place for

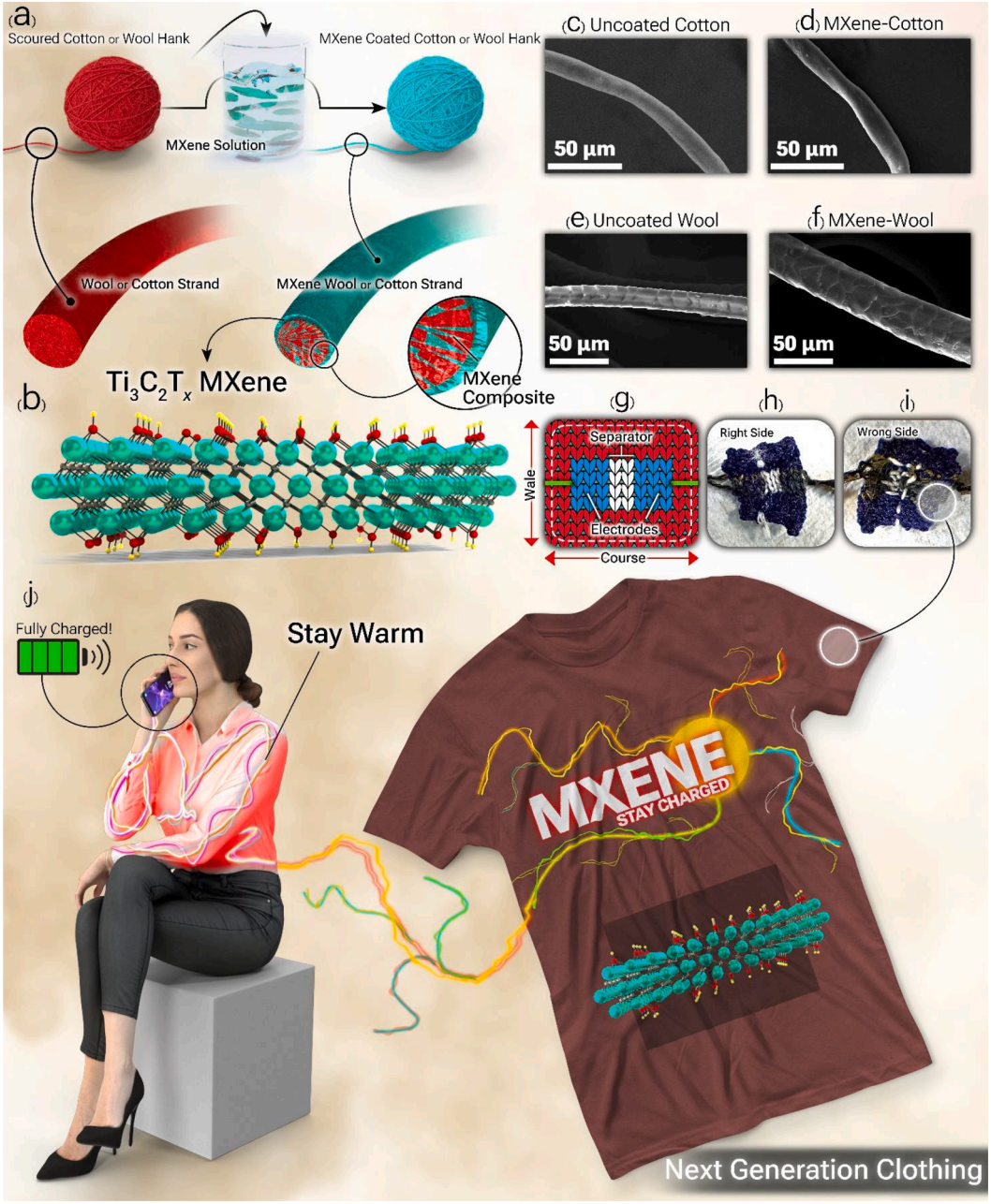

Fig. 1. a) Showing the coating of MXene flakes on cotton or wool yarn; b) Ti3C2TX MXene flake atomic structure; SEM images of c) uncoated cotton; d) MXene-coated cotton; e) uncoated wool; f) MXene-coated wool; g) geometry of knitted TSC with course and wale directions defined; h) right side of knitted TSC; i) wrong side of knitted TSC; j) conceptual design of smart energy storing garment.

electrochemical testing during strain (demonstration in Fig. S1a). Before performing the electrochemical characterization under mechanical stress, the TSCs were either folded (demonstration in Fig. S1c), stretched to 1.3 times their course width, or stretched to 1.2 times their wale length (demonstration in Fig. S1b) 100 times. TSC dimensions were measured after this repeated stretching to determine any deformation. Fig. 1g shows the orientation of the course and wale of the TSCs.

The electrochemical performance of TSCs under relaxed conditions and various mechanical deformation conditions was measured. Cyclic voltammograms were recorded at 50, 20, 10, 5, and 2 mV/s scan rates. The EIS measurements were conducted from 500 kHz to 0.1 Hz at an applied sinusoidal voltage of 10 mV. GCD experiments were conducted at current densities ranging from 1 to 3 mA/cm^2. GCD curves were cycled 1000 times to determine TSC cycle life for all the different tests. All results were compared to those of the control cotton and wool TSCs.

Tensile strength analysis

One 15-inch-long uncoated cotton and wool yarn, and two 15-inch long MXene-coated cotton and wool yarns were mounted in an Instron Tensile Tester following the standard test method for tensile properties of yarns by the single-strand method (ASTM D2256). Yarns were conditioned overnight to achieve moisture equilibrium prior to testing.

Leaching analysis using UV–Vis spectrophotometer

The leaching analysis involved investigating the leaching of MXene from cotton and wool yarn. In order to assess the release behavior and magnitude of MXene leaching from these textile materials, two 15-inch long MXene-coated cotton and wool yarn samples were initially weighed. They were then subjected to a sonication process in 10 mL of deionized (DI) water for a duration of 1 hour. Subsequently, the yarns were dried overnight under continuous vacuum, and their weights were measured again to determine the post-washing weight. The DI water used in the process was collected, and the amount of MXene flakes that detached from the yarn during washing was determined using a GENESYS™ 10 UV–Vis spectrophotometer. To establish a calibration curve, MXene solutions with concentrations ranging from 0.00125 to 0.02 mg/mL were prepared. The absorbance of each solution was measured at a wavelength of 770 nm using the UV–Vis spectrophotometer.

Data analysis

EIS was used to determine the resistive behavior of the device as well as to determine the equivalent circuit model (ECM) based on the measured impedance values. Eq. 1 was used to determine the equivalent capacitor:

$$Z = (2\pi fjC)^{-1} \tag{1}$$

where Z is the measured impedance, j is the square root of -1 (unit imaginary number), f is the frequency at which that data point was measured, and C is the capacitance. The equation can be solved for C to determine the capacitance of the ECM.

GCD was used to determine the cycle life of the TSCs. Specific capacitance was calculated using Eq. 2:

$$c = \frac{I\Delta t}{\Delta V} \tag{2}$$

Where C is the specific capacitance, I is the applied discharge current, Δt is the discharge time, and ΔV is the change in voltage during discharge.

Energy density was calculated using Eq. 3:

$$E = 0.5CV^2 \tag{3}$$

Where C is the specific capacitance and V is the change in discharge voltage.

Power density was calculated using Eq. 4:

$$P = \frac{E}{t} \tag{4}$$

Where E is the specific energy and t is the discharge time.

Gamry Echem Analyst software was used to generate equivalent circuit models (ECMs), fit them to the measured EIS results, and generate values for the different electrical components.

The percent elongation was calculated using Eq. 5:

$$E = \frac{\Delta L}{L_i} \times 100 \tag{5}$$

Where E is the elongation at breakage, ΔL is the difference between the final length and the initial length of the yarn being tested, and L is the original length of the yarn.

Results and discussion

Fig. 1a presents the coating of MXene on the cotton or wool yarn with MXene flakes penetrating the yarn to coat individual fibers in addition to covering the yarn surface. Fig. 1b presents the MXene structure with layers of carbon in between layers of titanium with oxide or fluoride surface terminations. Fig. 1c and d show the SEM image of uncoated and MXene-coated cotton fiber; prior to coating the smooth, ribbon-like surface of the cotton fiber is apparent, and after coating a slight increase in roughness on the cotton fiber surface can be observed. Fig. 1e and f present SEM images of uncoated and MXene-coated wool fiber; the rough surface caused by the outer cuticle of wool fibers is apparent in these images, as is a slight increase in roughness on each cuticle scale after coating the wool yarn with MXene flakes. Furthermore, the MXene has filled some of the spaces in between the fibers in the yarn, which increases the conductive network by interconnecting adjacent fibers. The mass loading of MXene flakes on cotton yarn was 4% and the mass loading of MXene flakes on wool yarn was 7%. We attribute the difference in the mass loading to the surface chemistry of the two fibers. The presence of nitrogen and sulfur in wool provides more surface charges, the main reason for the binding of pigment and dye particles with wool fibers. Hence, it is expected that the fiber surface of wool more readily binds with MXene flakes, leading to higher mass loading [23]. Wool fibers have an average surface charge of -23 mV at a pH of 6, and cotton fibers have an average surface charge of -14 mV at pH 10, and $Ti_3C_2T_x$ MXene flakes have a surface charge of -14.2 mV at a pH of 6. MXene nanosheets, similar to the way wool fibers interact with some dye molecules, form hydrogen bonds between the amino acid groups in wool and oxide surface terminations in MXene flakes, which can lead to a strong adherence. [14,37,45,65]

Fig. 1h and i show the front (hereafter referred to as the right side) and back (hereafter referred to as the wrong side) of a completed TSC with black electrodes, a white electrode separator, and navy fashion yarn surrounding the circuit. Fig. 1h clearly shows the stockinette stitch, achieved by knitting alternating rows of garter stitches on odd rows and purl stitches on even rows. The stockinette stitch is noted for its characteristic curling at the start and end of knitted textiles and can be seen at the top and bottom of Fig. 1h. Fig. 1g shows the intarsia knitting technique used to create color blocks in knit fabric while isolating the yarn to that area. If the yarn was carried across as practiced in double knitting (knitting with two or more strands of yarn), then the conductive electrodes would have a short circuit. In this image, the white electrode separator is clearly visible on the right and wrong sides of the TSC due to the intarsia knitting technique, meaning that the knitted electrodes are isolated from each other for electrochemical testing. The average size of cotton TSCs was 0.284 cm^2 and the average electrode separation was 3.8 mm. On the other hand, the average size of wool TSCs was 0.358 cm^2 and the average electrode separation was 2.3 mm. In other words, wool TSCs were 1.3 times larger than cotton TSCs, but cotton TSCs had nearly

twice the separation distance between the electrodes compared to wool TSCs.

Table 1 presents the results of tensile testing. The data shows that there is little difference in the maximum load or load at break between coated and uncoated samples. However, cotton exhibited a higher maximum and break load compared to wool, while wool showed a longer extension than cotton. The percent elongation for cotton was 5.33%, which is comparable to the literature. [10] For wool, it was 9.62%, slightly lower than the reported values. [10] This difference can be attributed to the relatively thinner yarns used in this research. The coated samples showed a much higher elongation before breaking. MXene coated cotton exhibited a 7.1% elongation, whereas MXene coated wool showed a 23.9% elongation. These findings indicate that the MXene coating improved the mechanical properties of the yarns which is in line with previous reports. [10,55]

Fig. 2a and b show the XPS spectra for uncoated and MXene-coated cotton and wool yarns. The XPS survey for uncoated cotton yarn indicates prominent carbon and oxygen peaks as these elements are the primary components of cotton fibers. The XPS survey shown in Fig. 3b for uncoated wool yarn also shows peaks for nitrogen and sulfur, as wool contains these elements in addition to carbon and oxygen. For the MXene-coated cotton and wool, the carbon peaks are less intense than their uncoated counterparts because the MXene flakes are covering the fiber and thus limiting the probing depth. $Ti_3C_2T_x$ MXene flakes are also constructed by layers of carbon in between layers of titanium, further decreasing the amount of carbon that will be detected by this method of surface characterization. This observation also explains the absence of nitrogen and sulfur peaks in the survey spectrum of the Mxene-coated wool yarn. MXene-coated cotton and wool yarn show prominent fluoride and titanium peaks due to the presence of the $Ti_3C_2T_x$ MXene flakes. Table 2 shows the atomic percentages of MXene-coated cotton and wool yarns from the XPS surveys.

The percentage of titanium and fluorine from the survey spectrum showed a slightly higher concentration of these elements on the MXene-coated cotton yarn. A small amount of nitrogen is still present in the coated wool samples and can be attributed to the presence of nitrogen in the wool fibers. The C1s and Ti2p atomic ratio does not corroborate with the stoichiometry of the MXene, which can be attributed to the fact that the MXene coating partially covers the yarns, and the signal from the substrate can be detected. The substrate, primarily composed of carbon and oxygen for both wool and cotton, can still be detected in areas where the conductive coating is thinner; as a result, carbon and oxygen have the largest atomic percentages in Table 1. Nitrogen and sulfur have minimal or no contribution to the atomic percentage of the MXene-coated wool fiber surface because these elements are preferential binding sites on wool fibers and are buried under the Mxene coating. [43]

Fig. 2c and d show the high-resolution Ti2p spectra for MXene-coated cotton and wool fiber, respectively. The spectra feature two distinct peaks separated by 5–6 eV of energy. These peaks can be deconvoluted in order to determine the chemical bonds at the surface of the sample, in this case $Ti_3C_2T_x$. [6,40] In the wool Ti2p scan, there were two distinct peaks at ~455 eV for the $Ti2p_{3/2}$ orbital and ~462 eV for the $Ti2p_{1/2}$ orbital; these two peaks were deconvoluted and each individual peak assigned to a chemical bonding. The peaks in the wool Ti2p scan at 455 and 460.7 eV were allocated to the Ti-C bond. The peaks at 455.8 and 461.8 eV can be related to the Ti(II) chemical state and the peaks at 457 and 462.7 eV can be specified to Ti(III). The peaks at 458.6 and 464.2 were allotted to Ti(IV) (TiO2), and the peaks at 459.3 and 465.3 eV correspond to the Ti-F chemical bonds. In the cotton Ti2p scan, there were again two distinct peaks at 455 eV for the $Ti2p_{3/2}$ orbital and 463 eV for the $Ti2p_{1/2}$ orbital. The deconvoluted peaks can be ascribed to the same chemical bonds and states as in the wool Ti2p scan. The peaks at 454.86 and 460.86 eV were related to the Ti-C chemical bond. The peaks at 455.53 and 461.53 were ascribed to the Ti (II), while the peaks at 456.53 and 456.62 eV were allocated to the Ti(III) oxidation state. The peaks at 457.97 and 464.02 eV were assigned to the Ti(IV) (TiO_2), and the peaks at 459.6 and 466.2 eV can be related to the Ti-F bond. [16,39] The oxidized peak is much more intense in the cotton Ti2p spectra than in the wool, likely due to the breathable nature of cotton fibers, whereas wool is insulating and is protecting the MXene flakes from oxidizing [23].

EDS was used to obtain further information about the composition of the samples, and the elemental mappings of the two yarns were compared (Fig. 3). As shown in Fig. 3, the sulfur and nitrogen signals can only be observed in Mxene-coated wool yarn, while both titanium (Ti) and fluorine (F) signals are clearly discernible on the surface, present on each fiber, and uniformly along their length.

Fig. 4 illustrates the UV–Vis absorbance of MXene solutions with various concentrations, the corresponding calibration curves used for quantifying MXene content in the leachate is shown. The MXene material demonstrated a distinctive absorption peak at 770 nm, consistent with previous reports. [50] Utilizing the calibration curve (Fig. S2), the estimated leachate of MXene from cotton was determined to be 0.00186 mg/mL, while from wool it was measured at 0.00255 mg/mL respectively.

Fig. 5 shows the specific capacitance of cotton and wool TSCs at various scan rates. Cotton outperformed wool at slower scan rates, but this gap decreased with increasing scan rates.[23] Fig. 5 a and b shows the CV curves of cotton- and wool-based TSCs at various scan rates. Cotton TSCs have a wider current range but greater resistive behavior while wool TSCs have a smaller current range but more pseudocapacitive behavior. The increased resistive behavior observed in the cotton TSCs is likely due to the decreased mass loading of MXene flakes on the yarns, larger electrodes, and wider electrode spacing. Compared to the cotton TSCs, the wool TSCs on average present a larger area, presenting a higher resistive behavior. This can explain the reduction in the measured current window of the voltammograms. The latter has a direct effect on the capacitive behavior of the fabricated capacitor and explains the differences in the specific capacitance in Fig. 5c and the specific areal capacitance in Fig. 5d. [28] There are a few reasons that explain why wool displays more pseudocapacitive behavior than cotton TSCs despite the larger electrodes. First, the electrode separation in wool TSCs was smaller than cotton TSCs, so ions in the electrolyte had a decreased distance to travel. Additionally, wool adsorbs more moisture than cotton, so wool TSCs adsorbed more aqueous electrolyte than cotton TSCs, improving the redox reactions occurring on the surface of the MXene flakes attached to the wool fibers [23,41].

Fig. 5e shows the GCD curves of cotton and wool TSCs at various current densities. At higher current densities and low measured voltage, GCD curves are linear in shape, indicating the EDLC behavior of the circuit. At higher voltages and lower current densities, GCD curves show significant deviation from linear behavior, indicating the pseudocapacitive behavior at the electrode surface. [54,57] Wool TSCs had more rapid charging and discharging behavior than cotton TSCs due to the absorption capabilities of wool fibers. The helical shape of wool yarn

Table 1
Breaking load, maximum load, and elongation of uncoated and MXene-coated cotton and wool yarn.

	Maximum Load (N)	Extension at Maximum Load (mm)	Load at Break (N)	Extension at Break (mm)	% Elongation
Uncoated cotton	19.77	20.37	19.75	20.4	5.33
MXene-coated cotton	19.91	27.03	19.9	27.1	7.08
Uncoated wool	10.64	35.56	10.11	36.8	9.62
MXene-coated wool	11.99	90.93	11.9	91.59	23.9

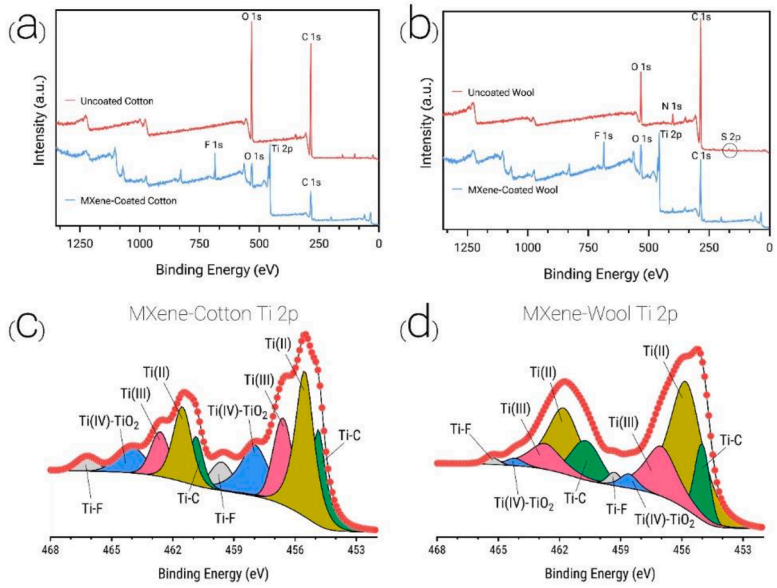

Fig. 2. XPS surveys of MXene-coated and uncoated a) cotton and b) wool yarn; high-resolution Ti2p spectra of MXene-coated c) cotton and d) wool yarn.

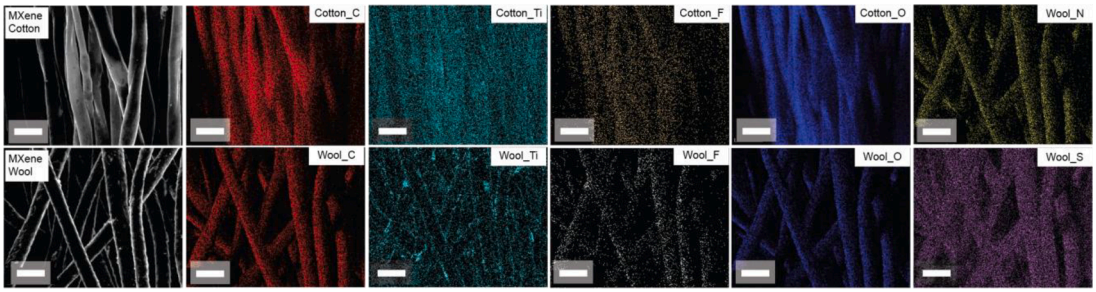

Fig. 3. EDS elemental mapping of MXene-coated cotton and MXene-coated wool yarn. The scale bar is 20 μm.

Table 2
Atomic percentages from XPS scans of MXene-coated cotton and wool yarn.

Element	Cotton	Wool
Ti2p	13.26	8.05
C1s	46.59	56.78
O1s	13.62	13.09
F1s	6.14	4.62
N1s	N/A	1.86

also results in more inter-fiber contact points, creating more pathways for electrons to move through the path of least resistance [23,28]. Fig. 5f shows the capacitance retention of cotton and wool TSCs during GCD cycling to determine cycle life of cotton and wool TSCs. After 1000 cycles, the capacitance retention of cotton TSCs remains steady, while the capacitance retention of wool TSCs starts to decline after approximately 1000 cycles. It is believed that the aqueous phosphoric acid electrolyte used was the cause of the degradation by hydrolyzing the cellulose in the cotton substrate. [1,11,13,42] Aqueous acidic environments similarly react to the wool substrate by breaking the disulfide bonds present in wool fibers, which explains the decline in discharge capacity in wool fibers [17,18,30].

Table 3 compares the calculated values of IR drop, areal capacitance, energy density, and power density of cotton and wool TSCs at various current densities. Cotton TSCs achieve a maximum energy density of 4.39 μWh/cm2 at 1 mA/cm^2 current density, and a peak power density of 0.44 mW/cm^2 at a current density of 3 mA/cm^2. For wool TSCs, peak energy density was 3.67 μWh/cm^2 at a 1 mA/cm^2 current density, and

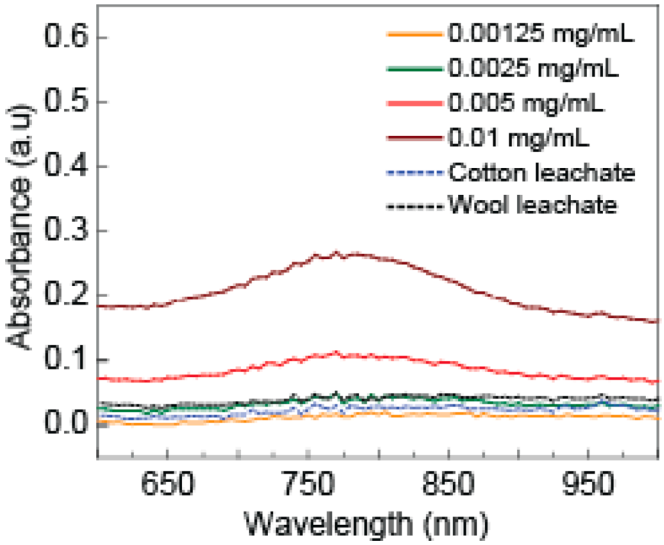

Fig. 4. UV–Vis absorption spectra of MXene at different concentrations for cotton and wool leachate.

had a maximum power density of 0.39 mW/cm^2. The maximum areal capacitance occurred with a current density of 1 mA/cm^2 where wool TSCs achieved 152.8 mF/cm^2 while cotton TSCs achieved 171.9 mF/cm^2; these values are comparable to the capacitance calculated from the

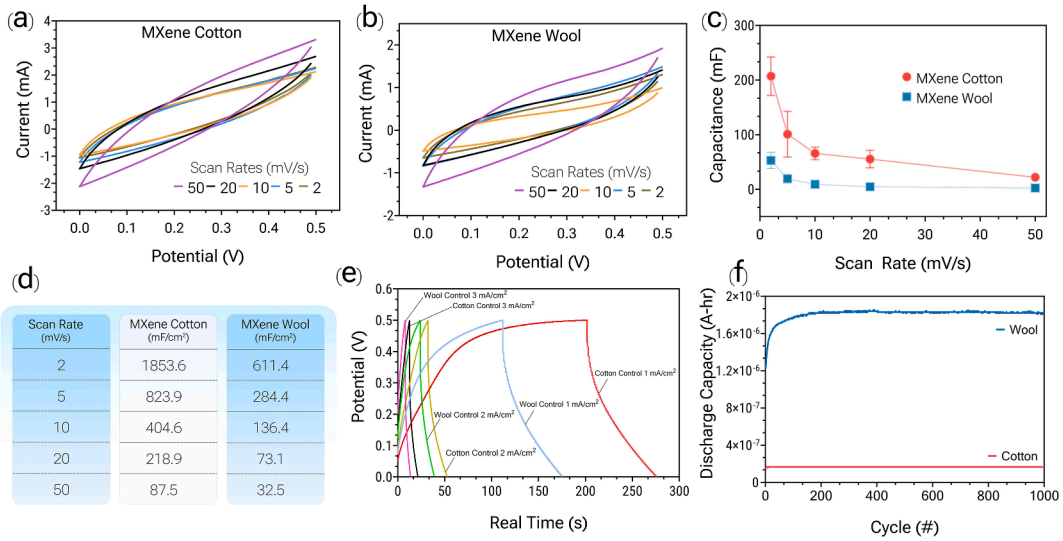

Fig. 5. CV curves of a) cotton and b) wool TSCs at various scan rates; c) specific capacitance of cotton and wool TSCs at various scan rates; d) a table of values calculated for the specific areal capacitance of cotton and wool TSCs; e) GCD curves of cotton and wool at various current densities; f) CDC cycles of cotton and wool TSCs to compare cycle life of the two substrates.

Table 3
IR drop, areal capacitance, energy density, and power densities of cotton and wool TSCs.

Current Density (mA/cm^2)	Cotton IR drop (mV)	Wool IR drop (mV)	Cotton Areal Capacitance (mF/cm^2)	Wool Areal Capacitance (mF/cm^2)	Cotton Energy Density (μWh/cm^2)	Wool Energy Density (μWh/cm^2)	Cotton Power Density (mW/cm^2)	Wool Power Density (mW/cm^2)
1	71.3	74.3	171.9	152.8	4.39	3.67	0.21	0.21
2	164.3	164.3	112.9	88.7	2.04	1.38	0.36	0.34
3	203.5	242.7	88	63.2	1.07	0.59	0.44	0.39

CV curves at various scan rates. The wool TSCs have a small IR drop of 74 mV at a 1 mA/cm^2 current density while for cotton this value is 71 mV. The calculated energy and power densities for cotton and wool TSCs are comparable to those reported in the literature [3,35,51].

Fig. 6a shows the EIS curves of cotton and wool TSCs. Both graphs feature a semicircle followed by a linearly increasing line. Wool TSCs have a higher resistance attributed to the electrolyte than cotton TSCs, and have a higher impedance ascribed to the capacitor overall. Wool has a rougher surface than cotton, so this creates a weaker contact point on the electrode surface during electrochemical testing, resulting in higher resistive behavior [23,41].

Fig. 6b shows the ECMs for cotton and wool-based TSCs and how well these models fit the measured EIS data. The equivalent capacitance in the measured data is the capacitance produced by the electrical double layer, consisting of the Stern and diffuse layers that must be modeled separately in an ECM. For both cotton- and wool-based TSCs, the equivalent capacitance for each component of the double layer is represented with constant phase elements (CPEs) labeled with Y, where a is the measure of ideal behavior for each capacitor with a value from 0 to 1, with 1 being ideal and 0 being non-ideal. R_s indicates the equivalent series resistance representing the resistances contributed by the electrode separation distance and the contact between the electrode and current collector, determined by the x-intercept on the EIS graph. R_{ct} is the resistance attributed to the charge transfer between the electrode surface and the electrolyte, connected in parallel with a CPE representing the capacitance contributed by the Stern layer, and calculated by extrapolating the arc of the EIS curve to form a second x-intercept. [25,46] The CPE in series with the rest of the ECM is representative of the capacitance contributed by the diffuse layer. [20,52] These CPEs indicate a non-ideal contact as a result of a three-dimensional electrode surface. [26] Fig. 6c compares the values calculated for the equivalent circuit components of cotton and wool TSCs using the ECM from Fig. 5b. [41,52,59] The equivalent resistor values for wool are ~30% higher than those generated for cotton. Wool also has lower equivalent capacitance values than cotton.

Fig. 7a-h displays the results of cotton and wool TSCs for CV curves measured at 50 mV/s, EIS curves, GCD curves at 1 mA/cm^2, and discharge capacities, respectively, under various deformations and compares them to the pristine or control TSCs. There were differences in TSC performance in response to washing or different deformation treatments depending on the electrode substrate; these differences are attributed to the differences in the structure and properties of the fibers and yarns. For all testing conditions, wool and cotton TSCs had non-linear triangular GCD curves indicative of pseudocapacitive behavior at the electrode surface [23,57].

Electrochemical tests were conducted on cotton and wool TSCs during course-wise stretching to compare their performance to the control TSCs. The CV curve in Fig. 7a for cotton TSCs had a slightly wider current range. The EIS curve in Fig. 7c shows an increased series resistance attributed to the increased electrode spacing and a smaller arc indicating a decreased charge transfer resistance. The GCD curve in Fig. 7e presents a more rapid charge and discharge trend with a larger IR drop. The faster charge and discharge cycles are attributed to tighter contact points when the yarns are stretched, allowing for more efficient electron transport. [15,25,36,54] The CV curve in Fig. 7b for wool TSCs tested under continuous course-wise stretching is virtually identical to the control, and in the EIS curve from Fig. 7d it can be observed that the series resistance is the same as the control due to the unchanging electrode separation distance. The electrodes of the wool TSCs remain at the same separation distance despite the course-wise stretching because of the different yarn twists between the electrode and separator yarn. The separator yarn is a loosely spun filament yarn with low twist while the electrodes use a higher twist wool yarn; as a result, most of the stretching along the course was contributed by the deformation of the wool yarn

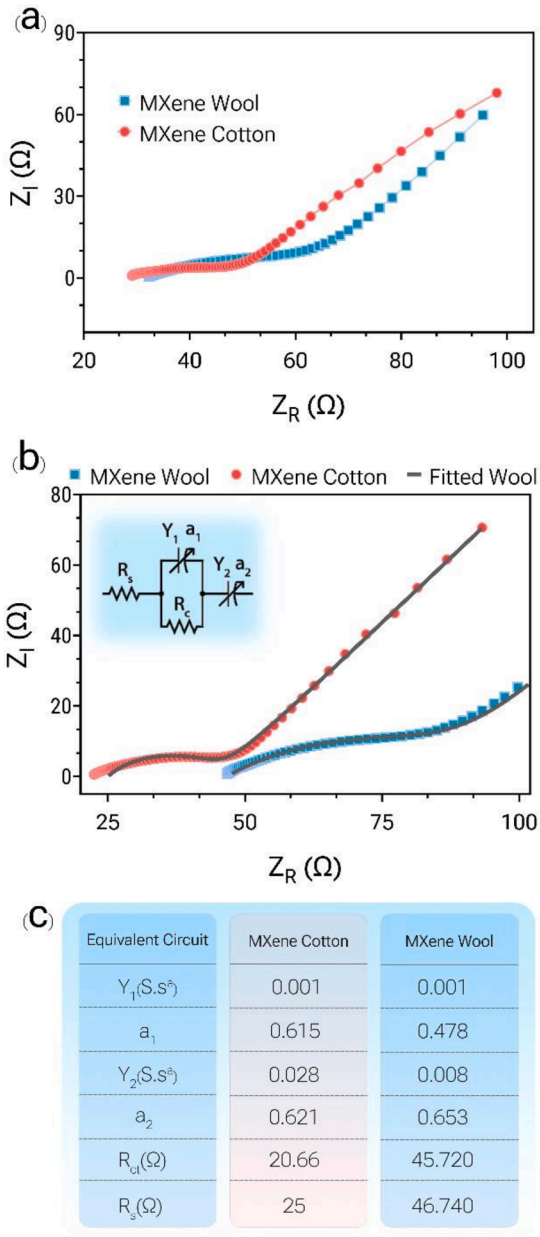

c

Equivalent Circuit	MXene Cotton	MXene Wool
Y_1(S.s^a)	0.001	0.001
a_1	0.615	0.478
Y_2(S.s^a)	0.028	0.008
a_2	0.621	0.653
R_{ct}(Ω)	20.66	45.720
R_s(Ω)	25	46.740

Fig. 6. a) average EIS measurements of cotton and wool TSCs; b) modeled data from the ECM shown overlaid on measured EIS data with an inset of an ECM; c) table of calculated equivalent circuit values for cotton and wool ECM TSCs.

with comparatively little change in the polyester separator yarn. The GCD curve in Fig. 7f depicts a longer charge/discharge time than pristine wool TSCs and can be attributed by a decreased number of inter-yarn contact points as a result of the yarn tightening under tension and opening up the yarn loops [5,15,23].

The same electrochemical tests were performed on cotton and wool TSCs after repeated course-wise stretching. The effect of repeated course-wise stretching on the electrochemical performance on cotton and wool TSCs were observed by running the same tests. Cotton TSCs had an increased current range in their CV curves compared to the control cotton TSCs, shown in Fig. 7a. There was a corresponding decrease in the series and charge transfer resistances as shown in Fig. 7c attributed to an increased number of contact points of the knitted structure from shifting fibers as a result of repeated stretching. These fibers shifting within the textile also contribute to the decreased maximum voltage in the GCD curve shown in Fig. 7e. Under the same testing conditions, the CV curves for wool in Fig. 7b have a slightly narrower current range and a higher charge transfer resistance in the EIS curves from Fig. 7d than that of pristine wool TSCs. These effects on the electrochemical behavior are attributed to the shifting wool fibers caused by repeated stretching. The GCD curves in Fig. 7f show a longer charge and discharge time due to the movement of the fibers during repeated deformation prior to testing. [5,15,28]

The same electrochemical tests were performed on cotton and wool TSCs during continuous wale-wise stretching. Cotton TSCs tested during this deformation test resulted in wider CV curves shown in Fig. 7a. There was a decreased charge transfer resistance in the EIS curves from Fig. 7c. The GCD results show a decreased charge/discharge time in the GCD curve attributed to an increased number of contact points of the conductive yarn with itself, thus increasing the number of pathways available to electrons in the TSC as a result of the continuous wale-wise stretching. [15,28] Wool TSCs tested under these conditions had similar CV results compared to the pristine wool TSCs as shown in Fig. 7a. There was a decreased series resistance as shown in the EIS curve in Fig. 7d due to the individual yarn loops deforming uniformly during stretching due to loop sizes being the same across different yarns, decreasing the electrode spacing. The GCD curves for continuously wale-wise stretched wool TSCs have a longer charge and discharge time than pristine TSCs shown in Fig. 7f, attributed to the deformation of the TSC during testing. [5,15,26]

Cotton and wool TSCs were stretched repeatedly in the wale direction prior to electrochemical testing to compare their performance to the control TSCs. Fig. 7a shows the CV curve for cotton TSCs has a wider current range than pristine cotton TSCs, while the EIS results in Fig. 7c have a lower charge transfer resistance. These results could be due to an increased number of inter-fiber contacts as a result of the repeated deformations, causing fibers to shift within the TSC. This allows for more efficient movement of ions through the electrode. The GCD curve in Fig. 7g for cotton TSCs under the same testing conditions displays faster charge and discharge than the pristine cotton TSCs, showing the more efficient movement of electrons through the conductive fabric. Fig. 7b shows the CV curve results for wool TSCs under the same testing conditions have a wider current range than pristine wool TSCs. Figure 7d shows the EIS results for wool TSCs have a lower series resistance that can be attributed to the decreased electrode spacing caused by repeated deformation in the wale-wise direction. This deformation also explains the longer GCD charge and discharge times shown in Fig. 7f. [5,15,28]

Cotton and wool TSCs were tested for their electrochemical performance after repeated folding and compared to the control TSCs; this type of repeated deformation in textiles usually results in fibers shifting within the textile. Fig. 7a shows the CV curve for cotton TSCs tested after repeated folding has a wider current range compared to pristine cotton TSCs and Fig. 7c shows that the corresponding EIS curve has a smaller charge transfer resistance. It can be observed that the GCD curve in Fig. 7g has a longer charge and shorter discharge time. These results are attributed to the fibers shifting within the knit fabric. Wool TSCs tested after repeated folding have a narrower current range in their CV curve than pristine wool TSCs as shown in Fig. 7b. The EIS results in Fig. 7d show that this treatment of wool TSCs increases the charge transfer resistance and increases the charge and discharge times of the corresponding GCD test as can be observed in Fig. 7f. Repeated folding causes a similar shift of fibers within the knitted wool, and explains the observed changes in the test results compared to the control. [5,15]

The results of cotton and wool TSCs that had been washed and dried prior to electrochemical tests were compared to the control TSCs; washing cotton and wool causes individual fibers to swell and shift within the yarns, and the changes in the results for the electrochemical tests are explained by this behavior. The CV curve in Fig. 7a for washed cotton TSCs shows a thicker curve and slightly wider current range than pristine cotton TSCs and is attributed to the swelling of cotton fibers as a result of washing. The EIS curve for washed cotton TSCs in Fig. 7c show a flatter EIS curve that is also attributed to the fibers swelling and moving from washing, resulting in a less ideal surface for the current

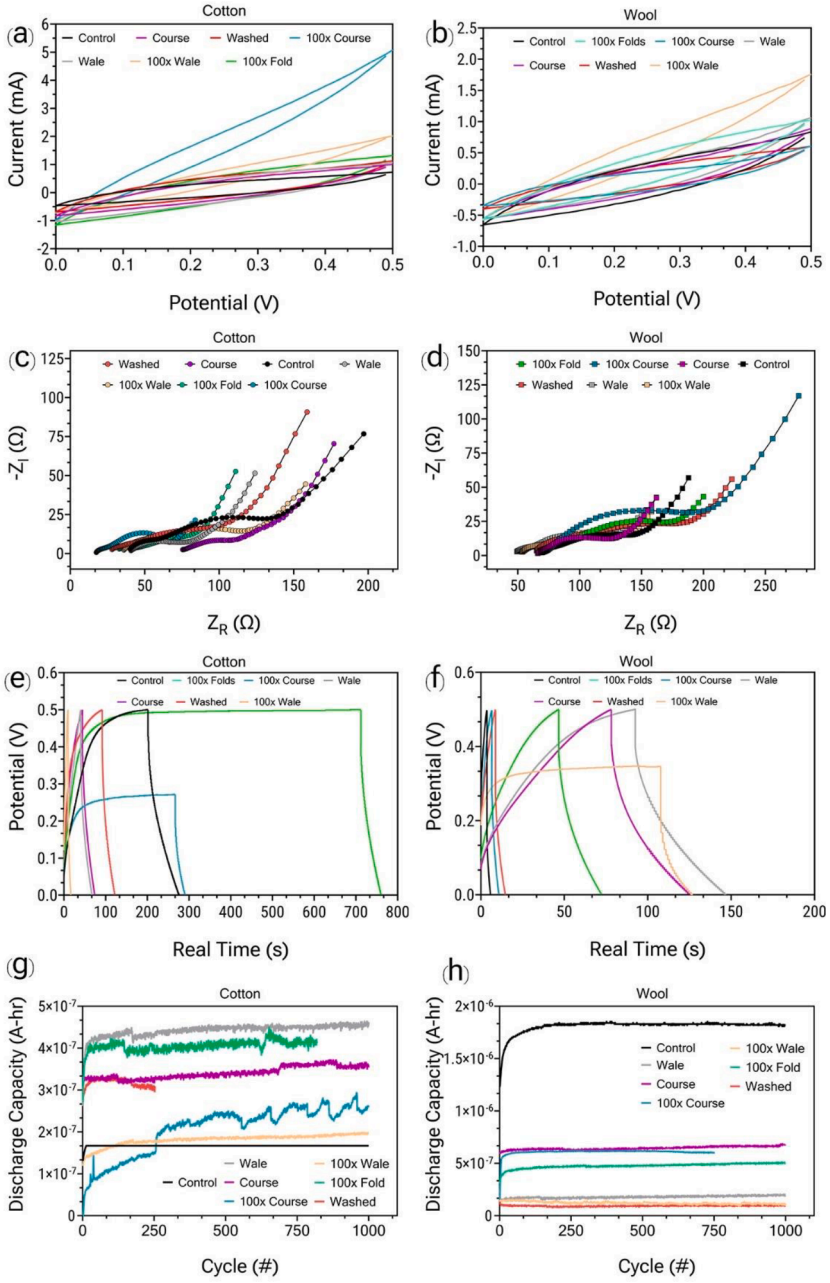

Fig. 7. CV curves of cotton (a) and wool (b) TSCs under various deformations at 50 mV/s scan rate; EIS curves of cotton (c) and wool (d) TSCs under various deformations; GCD curves of cotton (e) and wool (f) TSCs under various deformations and at various current densities; CDC cycling of cotton (g) and wool (h) TSCs under various deformations.

collector contact. The GCD curve for washed cotton TSCs in Fig. 7a had a faster change and discharge than pristine cotton TSCs, this is attributed to the fiber deformation. The CV curve in Fig. 7b of washed wool TSCs is similar to that of the pristine wool TSCs. The EIS curves shown in Fig. 7d of washed wool TSCs have flatter arcs and larger charge transfer resistances than pristine TSCs and can be attributed to the fibers swelling and shifting as a result of washing and causing less ideal contact with the current collector. The GCD curve for washed wool TSCs in Fig. 7f has a slower charging time than pristine TSCs attributed to the deformation of the wool fibers. [5,15]

Fig. 7g compares the discharge capacity up to 1000 cycles for cotton TSCs after various treatments to the control; likewise, Fig. 7h features the same comparison for wool TSCs. It can be observed that the discharge capacities for cotton TSCs were less stable than those of wool TSCs, likely due to the phosphoric acid hydrolyzing the cellulose present in the substrate for these TSCs. The dissolving substrate likely interfered with inter-fiber and inter-yarn interactions when cycling cotton TSCs during or after different deformations. The electrolyte does not cause this behavior in the wool TSCs because the disulfide bonds are cleaved at a slower rate by the weak phosphoric acid. Cotton TSCs that had been washed prior to cycling had decreased discharge capacity after 200 cycles attributed to the swelling of the cotton fibers from washing them [5,30,56]. Repeatedly folding cotton TSCs resulted in decreasing discharge capacity after approximately 700 cycles. Cotton TSCs tested after repeated course-wise stretching have decreased discharge capacity after approximately 600 cycles attributed to deformation of the knit loops interfering with inter-yarn contact points. Cycling after repeated wale-wise stretching results in slowly increasing discharge capacity explained by the yarn loops becoming tighter and increasing the number of inter-yarn contact points. Cotton TSCs that were tested during

stretching in the course or wale direction slowly increased in discharge capacity, likely due to the slower permeation of electrolyte into the yarns as a result of testing the TSCs under tension. Wool TSCs cycled during course-wise stretching, after repeated wale-wise stretching, and during wale-wise stretching had a slowly increasing discharge capacity attributed to the slow adsorption of electrolyte into the yarn, especially for the TSCs tested under tension. Wool TSCs tested after repeated course-wise stretching had a decreased discharge capacity after 500 cycles, likely caused by altered connections between the separator and electrode yarns as a result of repeated deformations. Wool TSCs that were cycled during continuous wale-wise stretching, after repeated wale-wise stretching, or after washing had a stable discharge capacity.

Conclusion

In this work, conductive protein-based yarns were prepared for TSCs by dip-coating wool fibers in $Ti_3C_2T_x$ MXene colloidal solution. The successful coating of the fibers with MXene flakes was verified by SEM-EDS and XPS analyses; then, the conductive yarn was knit into TSCs for electrochemical testing. The MXene-coated wool achieved a high specific capacitance of 284 mF/cm^2 at a scan rate of 5 mV/s, which proves that wool is a viable substrate for conductive materials in energy storage research and creates a new class of protein-based TSCs that utilizes the excellent adsorption properties of protein-based fibers such as wool. This new class of TSCs showed satisfactory electrochemical performance indicating wool is comparable to synthetic and cellulosic substrates. Electrochemical characterization indicated that the wool TSCs exhibited more pseudocapacitive behavior by improved interaction with the electrolyte at the fiber surface, while the cotton TSCs demonstrated a wider current range. GCD curves at different current densities show that wool TSCs have faster charge and discharge rates compared to cotton TSCs. This can be attributed to the better absorption of the liquid electrolyte by wool fibers. Cotton and wool TSCs were subjected to various tests, including washing, repeated folding, repeated course-wise and wale-wise stretching, as well as during course-wise and wale-wise stretching, to compare their performance. The physical deformation of cotton and wool TSCs did affect their electrochemical behavior, which can be attributed to the surface and tensile properties of the yarns used in their construction. This change in yarn tensile properties was confirmed through tensile testing, which showed improved elongation of the coated cotton and wool yarns before failure. Further exploration is required to increase the capacitance and reduce the resistance by altering the surface chemistry and functionalization of the MXene flakes.

Declaration of Competing Interest

The authors declare that they have no known competing financial interests or personal relationships that could have appeared to influence the work reported in this paper.

Acknowledgement

We acknowledge funding from NASA Nebraska Space Grant (UNL 26–389) and the University of Nebraska-Lincoln Research Council. The research was performed in part in the Nebraska Nanoscale Facility: National Nanotechnology Coordinated Infrastructure and the Nebraska Center for Materials and Nanoscience, which are supported by the National Science Foundation under Award ECCS: 1542182, and the Nebraska Research Initiative. The research was performed in part in the Labs for Functional Textiles and Protective Clothing at Iowa State University.

Supplementary materials

Supplementary material associated with this article can be found, in the online version, at doi:10.1016/j.nwnano.2023.100014.

References

[1] M.N. Amin, R.S. Blackburn, Sustainable chemistry method to improve the wash-off process of reactive dyes on cotton, ACS Sustain. Chem. Eng. 3 (2015) 725–732, https://doi.org/10.1021/acssuschemeng.5b00034.
[2] A. Arabi Shamsabadi, M. Sharifian, B. Anasori, M. Soroush, Antimicrobial mode-of-action of colloidal Ti3C2Tx MXene nanosheets, ACS Sustain. Chem. Eng. 6 (2018) 16586–16596, https://doi.org/10.1021/acssuschemeng.8b03823.
[3] Barakzehi, M., Montazer, M., Sharif, F., Norby, T., Chatzitakis, A., 2019. A textile-based wearable supercapacitor using reduced graphene oxide/polypyrrole composite. https://doi.org/10.1016/j.electacta.2019.03.058.
[4] V. Bhardwaj, A. Fairhurst, Fast fashion: response to changes in the fashion industry, The International Review of Retail, Distribution and Consumer Research, Int. Rev. Retail. Distrib. Consum. Res. 20 (2010) 165–173, https://doi.org/10.1080/09593960903498300.
[5] C. Billie, E. Helen, Textile testing and analysis, Prentice Hall, 1999.
[6] Y. Cao, Q. Deng, Z. Liu, D. Shen, T. Wang, Q. Huang, S. Du, N. Jiang, C.-T. Lin, J. Yu, Enhanced thermal properties of poly(vinylidene fluoride) composites with ultrathin nanosheets of MXene †, RSC Adv. (2017) https://doi.org/10.1039/c7ra00184c.
[7] B. Chessa, F. Pereira, F. Arnaud, A. Amorim, F. Goyache, I. Mainland, R.R. Kao, J. M. Pemberton, D. Beraldi, M. Stear, A. Alberti, M. Pittau, L. Iannuzzi, M. H. Banabazi, R. Kazwala, Y.-P. Zhang, J.J. Arranz, B.A. Ali, Z. Wang, M. Uzun, M. Dione, I. Olsaker, L.-E. Holm, U. Saarma, S. Ahmad, N. Marzanov, E. Eythorsdottir, M.J. Holland, P. Ajmone-Marsan, M.W. Bruford, J. Kantanen, T. E. Spencer, M. Palmarini, Revealing the history of sheep domestication using retrovirus integrations, Science (80-.) 324 (2009) 532–536, https://doi.org/10.1126/science.1170587.
[8] M. Dadashi Firouzjaei, M. Karimiziarani, H. Moradkhani, M. Elliott, B. Anasori, MXenes: The two-dimensional influencers, Mater. Today Adv. (2022), https://doi.org/10.1016/j.mtadv.2021.100202.
[9] B.L. Deopura, N.V. Padaki, Synthetic Textile Fibers: Polyamide, Polyester, and Aramid Fibers, Woodhead Publishing, 2015, https://doi.org/10.1016/B978-1-84569-931-4.00005-2.
[10] Y. Elmogahzy, R. Farag, Handbook of properties of textile and technical fibres, Woodhead Publishing, 2018.
[11] S.C. Espinosa, T. Kuhnt, E. Johan Foster, C. Weder, Isolation of thermally stable cellulose nanocrystals by phosphoric acid hydrolysis, J. Renew. Mater. 8 (2020) 187–203, https://doi.org/10.32604/jrm.2020.07940.
[12] M.D. Firouzjaei, S.K. Nemani, M. Sadrzadeh, E.K. Wujcik, M. Elliott, B. Anasori, Life cycle assessment of Ti 3 C 2 T x MXene synthesis, Adv. Mater. (2023), https://doi.org/10.1002/adma.202300422.
[13] K. Gourlay, V. Arantes, J.N. Saddler, Use of substructure-specific carbohydrate binding modules to track changes in cellulose accessibility and surface morphology during the amorphogenesis step of enzymatic hydrolysis, Biotechnol. Biofuels 5 (2012) 1–14, https://doi.org/10.1186/1754-6834-5-51.
[14] A.M. Grancaric, A. Tarbuk, S. Hadzic, B. Simoncic, From raw to finished cotton—characterization by interface phenomena, Autex Res. J. 0 (2022), https://doi.org/10.2478/aut-2021-0055.
[15] H. Gu, Y. Zeng, Q. Zhong, Y. Bu, Highly reversibly stretchable and elastically wearable textile supercapacitor, ACS Appl. Mater. Interfaces 15 (2023) 24448–24458, https://doi.org/10.1021/acsami.3c02306.
[16] Halim, J., Cook, K.M., Naguib, M., Gogotsi, Y., Rosen, J., Barsoum, M.W., n.d. X-ray photoelectron spectroscopy of select multi-layered transition metal carbides (MXenes). OSTI.
[17] M. Harris, A.L. Smith, Photochemical reactions of wool, J. Res. Natl. Bur. Stand. (1934) 20 (1938) 563, https://doi.org/10.6028/jres.020.022.
[18] M. Harris, A.L. Smith, State of the sulfur in oxidized wool, J. Res. Natl. Bur. Stand. 18 (1937) 623, https://doi.org/10.6028/jres.018.039, 1934.
[19] J. Hassoun, S. Panero, P. Reale, B. Scrosati, A new, safe, high-rate and high-energy polymer lithium-ion battery, Adv. Mater. (2009), https://doi.org/10.1002/adma.200900470.
[20] K. Hung, C. Masarapu, T. Ko, B. Wei, Wide-temperature range operation supercapacitors from nanostructured activated carbon fabric, J. Power Sources 193 (2009) 944–949, https://doi.org/10.1016/J.JPOWSOUR.2009.01.083.
[21] A.P. Isfahani, A. Arabi Shamsabadi, M. Soroush, MXenes and other two-dimensional materials for membrane gas separation: progress, challenges, and potential of MXene-based membranes, Ind. Eng. Chem. Res. 62 (2023) 2309–2328, https://doi.org/10.1021/acs.iecr.2c02042.
[22] A.P. Isfahani, A.A. Shamsabadi, F. Alimohammadi, M. Soroush, Efficient mercury removal from aqueous solutions using carboxylated Ti3C2Tx MXene, J. Hazard. Mater. 434 (2022), https://doi.org/10.1016/j.jhazmat.2022.128780.
[23] J.G. Cook, Handbook of textile fibers: natural fibers, 1984.
[24] K. Jost, D. Stenger, C.R. Perez, J.K. McDonough, K. Lian, Y. Gogotsi, G. Dion, Knitted and screen printed carbon-fiber supercapacitors for applications in wearable electronics, Energy Environ. Sci. 6 (2013) 2698–2705, https://doi.org/10.1039/C3EE40515J.
[25] J. Kang, J. Wen, S.H. Jayaram, A. Yu, X. Wang, Development of an equivalent circuit model for electrochemical double layer capacitors (EDLCs) with distinct electrolytes, Electrochim. Acta 115 (2014) 587–598, https://doi.org/10.1016/j.electacta.2013.11.002.
[26] C.H. Kim, S.Il Pyun, J.H. Kim, An investigation of the capacitance dispersion on the fractal carbon electrode with edge and basal orientations, Electrochim. Acta 48 (2003) 3455–3463, https://doi.org/10.1016/S0013-4686(03)00464-X.

[27] Lee, J.A., Fang, D.D., 2015. Cotton as a world crop: origin, history, and current status, in: Cotton. John Wiley & Sons, Ltd, pp. 1–23. https://doi.org/https://doi.org/10.2134/agronmonogr57.2013.0019.

[28] Levitt, A., Hegh, D., Phillips, P., Uzun, S., Anayee, M., Razal, J.M., Gogotsi, Y., Dion, G., 2020a. 3D knitted energy storage textiles using MXene-coated yarns. https://doi.org/10.1016/j.mattod.2020.02.005.

[29] Levitt, A., Zhang, J., Dion, G., Gogotsi, Y., Razal, J.M., Levitt, A., Gogotsi J., Dion, Y.A., Zhang, G., Razal, J., J M., 2020b. MXene-based fibers, yarns, and fabrics for wearable energy storage devices. https://doi.org/10.1002/adfm.202000739.

[30] B. Li, J. Yao, J. Niu, J. Liu, L. Wang, M. Feng, Y. Sun, Study on the effect of organic phosphonic compounds on disulfide bonds in wool, Text. Res. J. 89 (2019) 2682–2693, https://doi.org/10.1177/0040517518798652.

[31] M. Li, Z. Li, L. Qu, F. Chen, M. Tian, Recent progress of the active materials with various micro-structures for flexible textile-based supercapacitors, Adv. Fiber Mater. (2022).

[32] M. Li, Z. Li, X. Ye, W. He, L. Qu, M. Tian, A smart self-powered rope for water/fire rescue, Adv. Funct. Mater. 33 (2023), https://doi.org/10.1002/adfm.202210111.

[33] M. Li, Z. Li, X. Ye, X. Zhang, L. Qu, M. Tian, Tendril-inspired 900% ultrastretching fiber-based Zn-ion batteries for wearable energy textiles, ACS Appl. Mater. Interfaces 13 (2021) 17110–17117, https://doi.org/10.1021/acsami.1c02329.

[34] Z. Li, M. Li, Q. Fan, X. Qi, L. Qu, M. Tian, Smart-fabric-based supercapacitor with long-term durability and waterproof properties toward wearable applications, ACS Appl. Mater. Interfaces 13 (2021) 14778–14785, https://doi.org/10.1021/acsami.1c02615.

[35] Li, Z., Ma, Y., Wang, L., Du, X., Zhu, S., Zhang, X., Qu, L., Tian, M., 2019. Multidimensional hierarchical fabric-based supercapacitor with bionic fiber microarrays for smart wearable electronic textiles. https://doi.org/10.1021/acsami.9b19078.

[36] J. Lim, D.S. Choi, G.Y. Lee, H.J. Lee, S.P. Sasikala, K.E. Lee, S.H. Kang, S.O. Kim, Omnidirectional deformable energy textile for human joint movement compatible energy storage, ACS Appl. Mater. Interfaces 9 (2017) 41363–41370, https://doi.org/10.1021/acsami.7b14981.

[37] S. Mirnezhad, S. Safapour, M. Sadeghi-Kiakhani, Dual-mode adsorption of cochineal natural dye on wool fibers: kinetic, equilibrium, and thermodynamic studies, Fibers Polym. 18 (2017) 1134–1145, https://doi.org/10.1007/s12221-017-6923-3.

[38] M. Mozafari, A. Arabi Shamsabadi, A. Rahimpour, M. Soroush, Ion-selective MXene-based membranes: current status and prospects, Adv. Mater. Technol. 6 (2021), https://doi.org/10.1002/admt.202001189.

[39] L.Å. Naslund, P.O.Å. Persson, J. Rosen, X-ray photoelectron spectroscopy of Ti3AlC2, Ti3C2Tz, and TiC provides evidence for the electrostatic interaction between laminated layers in max-phase materials, J. Phys. Chem. C 124 (2020) 27732–27742, https://doi.org/10.1021/ACS.JPCC.0C07413.

[40] V. Natu, M. Benchakar, C. Canaff, A. Habrioux, S. Célérier, M.W. Barsoum, A critical analysis of the X-ray photoelectron spectra of Ti3C2Tz MXenes, Matter (2021), https://doi.org/10.1016/j.matt.2021.01.015.

[41] M. Orazem, B. Tribollet, Electrochemical impedance spectroscopy, 2017. Hoboken, New Jersey.

[42] S.N. Pandey, P. Nair, Effect of phosphoric acid treatment on physical and chemical properties of cotton fiber, Text. Res. J. (1973) 927–933.

[43] Pielesz, A., 2003. Characteristics of Azo-Dye Binding Sites on Wool-Fiber Keratin. https://doi.org/10.1002/app.13443.

[44] M. Rezakazemi, A. Arabi Shamsabadi, H. Lin, P. Luis, S. Ramakrishna, T. M. Aminabhavi, Sustainable MXenes-based membranes for highly energy-efficient separations, Renew. Sustain. Energy Rev. 143 (2021), https://doi.org/10.1016/j.rser.2021.110878.

[45] A. Rozmysłowska-Wojciechowska, J. Mitrzak, A. Szuplewska, M. Chudy, J. Woźniak, M. Petrus, T. Wojciechowski, A.S. Vasilchenko, A.M. Jastrzębska, Engineering of 2D Ti3C2 MXene surface charge and its influence on biological properties, Materials (Basel) 13 (2020), https://doi.org/10.3390/MA13102347.

[46] P. Saha, S. Dey, M. Khanra, Modeling and state-of-charge estimation of supercapacitor considering leakage effect, IEEE Trans. Ind. Electron. 67 (2020) 350–357, https://doi.org/10.1109/TIE.2019.2897506.

[47] F. Seidi, A. Arabi Shamsabadi, M. Dadashi Firouzjaei, M. Elliott, M.R. Saeb, Y. Huang, C. Li, H. Xiao, B. Anasori, MXenes antibacterial properties and applications: a review and perspective, Small (2023), https://doi.org/10.1002/smll.202206716.

[48] S. Senthilkannan Muthu, Y. Li, J. Hu, P. Mok, Quantification of environmental impact and ecological sustainability for textile fibres, Ecol. Indic. 13 (2012) 66–74, https://doi.org/10.1016/j.ecolind.2011.05.008.

[49] A.A. Shamsabadi, A.P. Isfahani, S.K. Salestan, A. Rahimpour, B. Ghalei, E. Sivaniah, M. Soroush, Pushing rubbery polymer membranes to be economic for CO2 separation: embedment with Ti3C2Tx MXene nanosheets, ACS Appl. Mater. Interfaces 12 (2020) 3984–3992, https://doi.org/10.1021/acsami.9b19960.

[50] C.E. Shuck, A. Sarycheva, M. Anayee, A. Levitt, Y. Zhu, S. Uzun, V. Balitskiy, V. Zahorodna, O. Gogotsi, Y. Gogotsi, Scalable synthesis of Ti3C2Tx MXene, Adv. Eng. Mater. 22 (2020) 1–8, https://doi.org/10.1002/adem.201901241.

[51] H.J. Sim, C. Choi, D.Y. Lee, H. Kim, J.H. Yun, J.M. Kim, T.M. Kang, R. Ovalle, R. H. Baughman, C.W. Kee, S.J. Kim, Biomolecule based fiber supercapacitor for implantable device, Nano Energy 47 (2018) 385–392, https://doi.org/10.1016/j.nanoen.2018.03.011.

[52] M.D. Stoller, C.W. Magnuson, Y. Zhu, S. Murali, J.W. Suk, R. Piner, R.S. Ruoff, Interfacial capacitance of single layer graphene, Energy Environ. Sci. 4 (2011) 4685–4689, https://doi.org/10.1039/C1EE02322E.

[53] Q. Sun, D. Yu, F. Mo, M. Wu, Y. Liu, X. Dong, Wool textile-derived nitrogen-doped porous carbon cloth for a binder-free electrode material for high-performance flexible solid-state supercapacitors, J. Mater. Sci. 56 (2021) 2412–2424, https://doi.org/10.1007/S10853-020-05314-X.

[54] S.K. Ujjain, R. Bhatia, P. Ahuja, P. Attri, Highly conductive aromatic functionalized multi-walled carbon nanotube for inkjet printable high performance supercapacitor electrodes, PLoS One 10 (2015) 1–12, https://doi.org/10.1371/journal.pone.0131475.

[55] S. Uzun, S. Seyedin, A.L. Stoltzfus, A.S. Levitt, M. Alhabeb, M. Anayee, C.J. Strobel, J.M. Razal, G. Dion, Y. Gogotsi, Knittable and Washable Multifunctional MXene-Coated Cellulose Yarns, Adv. Funct. Mater. 29 (2019), https://doi.org/10.1002/adfm.201905015.

[56] O.M. Vanderfleet, D.A. Osorio, E.D. Cranston, Optimization of cellulose nanocrystal length and surface charge density through phosphoric acid hydrolysis, Philos. Trans. R. Soc. A Math. Phys. Eng. Sci. 376 (2018), https://doi.org/10.1098/rsta.2017.0041.

[57] H. Vijeth, S.P. Ashokkumar, L. Yesappa, M. Niranjana, M. Vandana, H. Devendrappa, Flexible and high energy density solid-state asymmetric supercapacitor based on polythiophene nanocomposites and charcoal, RSC Adv. 8 (2018) 31414–31426, https://doi.org/10.1039/c8ra06102e.

[58] Wang, B., Wang, M., Liu, F., Zhang, Q., Yao, S., Liu, X., Huang, F., n.d. Photocatalysis Very Important Paper Ti 3 C 2 :AnIdeal Co-catalyst? https://doi.org/10.1002/anie.201913095.

[59] W. Xi, J. Jin, Y. Zhang, R. Wang, Y. Gong, B. He, H. Wang, Hierarchical MXene/transition metal oxide heterostructures for rechargeable batteries, capacitors, and capacitive deionization, Nanoscale 14 (2022) 11923–11944, https://doi.org/10.1039/D2NR02802F.

[60] Yang, E., Xu, Z., Chur, L.K., Behroozfar, A., Baniasadi, M., Moreno, S., Huang, J., Gilligan, J., Minary-Jolandan, M., 2017. Nanofibrous smart fabrics from twisted yarns of electrospun piezopolymer. https://doi.org/10.1021/acsami.7b06032.

[61] C. Yuning Meng, Yang Zhao, Chuangang Hu, Huhu Cheng, Y. Hu, Zhipan Zhang, Gaoquan Shi, Liangti Qu, Y. Meng, Y Zhao, C Hu, H Cheng, Z Zhang, L Qu, G Shi, All-graphene core-sheath microfi bers for all-solid-state, stretchable fibriform supercapacitors and wearable electronic textiles, Adv. Mater. (2013), https://doi.org/10.1002/adma.201300132.

[62] C. Zhan, M. Naguib, M. Lukatskaya, P.R.C. Kent, Y. Gogotsi, D.-E. Jiang, Understanding the MXene pseudocapacitance, J. Phys. Chem. Lett 9 (2018) 6, https://doi.org/10.1021/acs.jpclett.8b00200.

[63] C. Zhang, L. McKeon, M.P. Kremer, S.-H. Park, O. Ronan, A. Seral-Ascaso, S. Barwich, C. Ó Coileáin, N. McEvoy, H.C. Nerl, B. Anasori, J.N. Coleman, Y. Gogotsi, V. Nicolosi, A. Drexel, Additive-free MXene inks and direct printing of micro-supercapacitors, Nat. Commun. (2019), https://doi.org/10.1038/s41467-019-09398-1.

[64] X. Zhao, A. Vashisth, E. Prehn, W. Sun, S.A. Shah, T. Habib, Y. Chen, Z. Tan, J. L. Lutkenhaus, M. Radovic, M.J. Green, Antioxidants unlock shelf-stable Ti3C2Tx (MXene) nanosheet dispersions, Matter 1 (2019) 513–526, https://doi.org/10.1016/j.matt.2019.05.020.

[65] B. Zimmerman, J. Chow, A.G. Abbott, M.S. Ellison, M.S. Kennedy, D. Dean, Variation of surface charge along the surface of wool fibers assessed by high-resolution force spectroscopy, J. Eng. Fibres Fabr. (2011).